Received: 22 June 2022 | Revised: 4 January 2023 | Accepted: 23 February 2023

DOI: 10.1002/ppp.2183

RESEARCH ARTICLE

WILEY

Last Glacial Maximum cryogenic calcite deposits in an alluvial fan at Villetoureix, southwest France

Pascal Bertran[1,2] | Isabelle Couchoud[3,4] | Karine Charlier[5] | Christine Hatté[6,7] | Yannick Lefrais[8] | Nicole Limondin-Lozouet[9] | Alain Queffelec[2]

[1]Inrap, Bègles, France

[2]PACEA, UMR 5199 CNRS, University of Bordeaux, Pessac, France

[3]EDYTEM, UMR 5204 CNRS, University Savoie Mont Blanc, Le Bourget du Lac cedex, France

[4]School of Geography, Earth and Atmospheric Sciences, The University of Melbourne, Carlton, Victoria, Australia

[5]EPOC, UMR 5805 CNRS, University of Bordeaux, Pessac, France

[6]LSCE, UMR 8212 CEA-CNRS-UVSQ, University Paris-Saclay, Gif-sur-Yvette, France

[7]Institute of Physics - CSE, Silesian University of Technology, Gliwice, Poland

[8]Archéosciences-Bordeaux, UMR 6034 CNRS, University Bordeaux Montaigne, Pessac, France

[9]Laboratoire de Géographie Physique, UMR 8591 CNRS, University Paris 1, Thiais, France

Correspondence
Pascal Bertran, Inrap, 140 avenue du Maréchal Leclerc, 33130 Bègles, France.
Email: pascal.bertran@inrap.fr

Funding information
Institut national de recherches archéologiques préventives

Abstract

The origin of white calcite silts forming 0.5 to 3-cm-thick lenses in alluvial fan deposits ^{14}C-dated to the Last Glacial Maximum in the Dronne Valley (Dordogne, southwest France) is investigated using microscopic imagery, chemistry, and O and C stable isotopes. The calcite silts, composed mainly of aggregates of 3–5-μm euhedral crystals, do not resemble secondary precipitations of pedological origin because of the strata-like pattern and the lack of clearly identifiable biological structures. Their association with evidence of ice formation in the soil (platy structure, involutions) suggests that they were deposited in a deep seasonal frost context. Their isotopic composition differs significantly from those of detrital carbonates and of Holocene bioprecipitation and seems to be best explained by precipitation under closed-system conditions. Calculation of the isotopic composition of calcite that would have formed in equilibrium with groundwater of regional LGM aquifers provides values that are in the range of the composition of the calcite silts for a precipitation temperature close to 0°C. Therefore, these deposits are interpreted as cryogenic calcite precipitated from waters close to saturation with respect to calcite freezing at the base of/within icings or within the ground, possibly from frost blisters. Similar calcite precipitation at the outlet of karstic springs may have been abundant in the calcareous terrains of southwest France during the LGM, although still unrecognized in the geological record.

KEYWORDS
cryogenic calcite, icing, Last Glacial Maximum, malacofauna, O and C stable isotopes, southwest France

1 | INTRODUCTION

Over the past decade, mapping of field evidence of permafrost,[1] estimation of aquifer recharge temperature,[2] and paleoclimate modeling[3] have shown that the Aquitaine region (southwest France, 44–45°N) was not affected by permafrost during the Last Glacial Maximum (LGM). Periglacial environments associated with deep seasonal ground freezing nevertheless existed as demonstrated by a range of indicators, particularly ground thermal contraction cracks filled with aeolian sand (i.e., relict sand wedges[1,4]) and cryoturbation.[5] In this

context, different types of seasonal ice are likely to have existed in the ground and on the surface. They include segregation ice, intrusion ice, icings, and ice infills in caves. In most cases, these ice bodies did not leave readily identifiable traces after melting. A few exceptions involve lenses of segregation ice in soils (e.g.,[6]), which created platy (micro-)structures stable enough to be preserved over time. Platy structures have been identified throughout Aquitaine in LGM sediments (e.g.,[7,8]).

In calcareous environments, the formation of ice from mineralized water leads to oversaturation with respect to calcite and precipitation of "cryogenic calcite." The calcite crystals have a variable size and morphology depending on precipitation conditions, in particular air temperature, precipitation rate, and gas exchange (CO_2) with the atmosphere,[9–11] and depending on the depositional environment (ground or ice surface, pools, sediments).[10,12–14] Cryogenic calcite accumulations are well known in modern cold environments and have been the subject of a great deal of work. As such, when preserved in the sedimentary record, they are good indication of the presence of ice in the past. Pleistocene cryogenic calcite has been reported in the literature mainly from caves in Europe (e.g.,[10,15–17]). Subglacial calcite has also been described by Sharp et al.[18] and Lipar et al.,[19] while the only example of intra-sedimentary cryogenic calcite precipitation has been reported by Thiry et al.[13] in the Paris Basin, France.

The purpose of this paper is to describe white calcite silt lenses, interpreted as LGM cryogenic calcite deposits interbedded in an alluvial fan in Aquitaine discovered during the excavation of an archaeological site. It constitutes the first-known example in southwest France. After description of the geomorphological and stratigraphic setting, the arguments in favor of the cryogenic origin of the calcite deposits are presented.

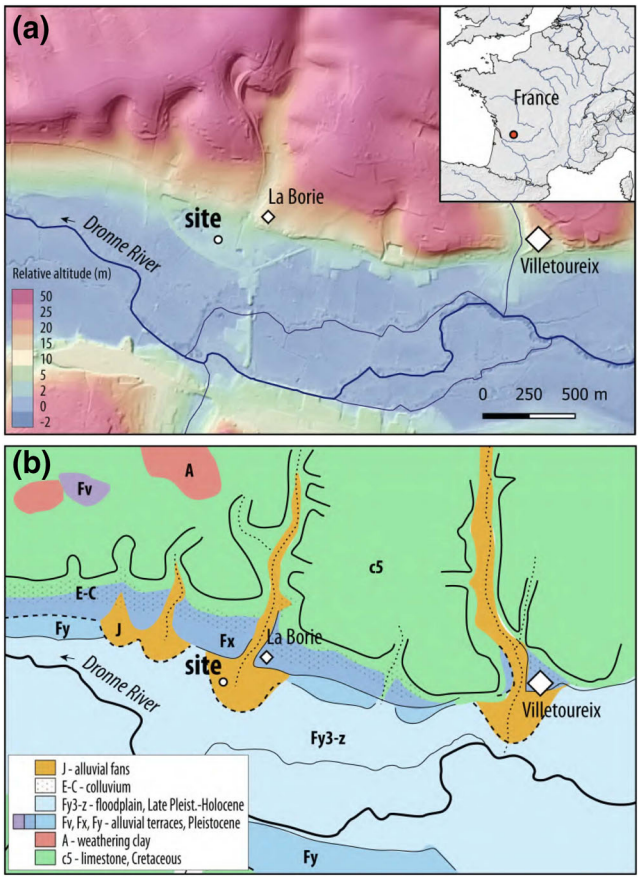

FIGURE 1 Location and geomorphological setting of the study site. A — Topography from Lidar survey (RGEALTI 5 m, Institut Géographique National); B — Geology, modified from the 1:50,000 digital geological map of France (https://infoterre.brgm.fr/). The labels of geological units are from Bourbon.[20] In (B), the longitudinal slope of the river has been subtracted from the digital elevation model, and the values indicated are altitudes relative to the riverbanks.

2 | GEOMORPHOLOGICAL SETTING

The site (0°20′25″E, 45°15′46″N, altitude ca. 61 m a.s.l.) is located in the Dronne Valley, on the right bank of the river 1.7 km west of the village of Villetoureix. The topography revealed by Lidar survey (RGEALTI® 5 m, Institut Géographique National) shows that it is located on an alluvial fan at the outlet of a dry valley incising the limestone bedrock (Campanian, 1:50000 geological map of France, https://infoterre.brgm.fr/) (Figure 1). The morphology of the main dry valley and the small tributary valleys, which start upstream in a cirque, suggests that water circulation through karst conduits largely contributed to the formation of the fan.

The alluvial fan extends over the plain of the Dronne River, which rises to approximately 58.5 m a.s.l. in the site area. The preliminary archaeological trenches[21] gave a general idea of the stratigraphy of QUATERNARY deposits. The main lithostratigraphic units identified (Camus and Rabanit, in[21]) are the following, from the base to the top:

1. Gravel deposited by the Dronne River, showing a lithology dominated by flint, limestone, and quartz, with rare magmatic and metamorphic rocks. The gravel layer was only reached by trenches in the distal part of the fan at a depth of 2 m, that is, around 56.5 m a.s.l.
2. Silty and sandy levels deposited by the alluvial fan, interbedded with lenses of limestone gravel in the upslope part of the surveyed piece of land.
3. A clayey level less than 1 m thick, mixed with abundant limestone clasts in the upper part. This level has yielded numerous Neolithic remains.

Work carried out later during the excavation of a Magdalenian level[22] buried at a depth of about 3 m in the fan made it possible to gather new observations on a limited area (35 m^2) and to collect dating elements.

3 | METHODS

During the excavation, detailed field observations were made on the available sections. As molluscan shells were visible to the naked eyes

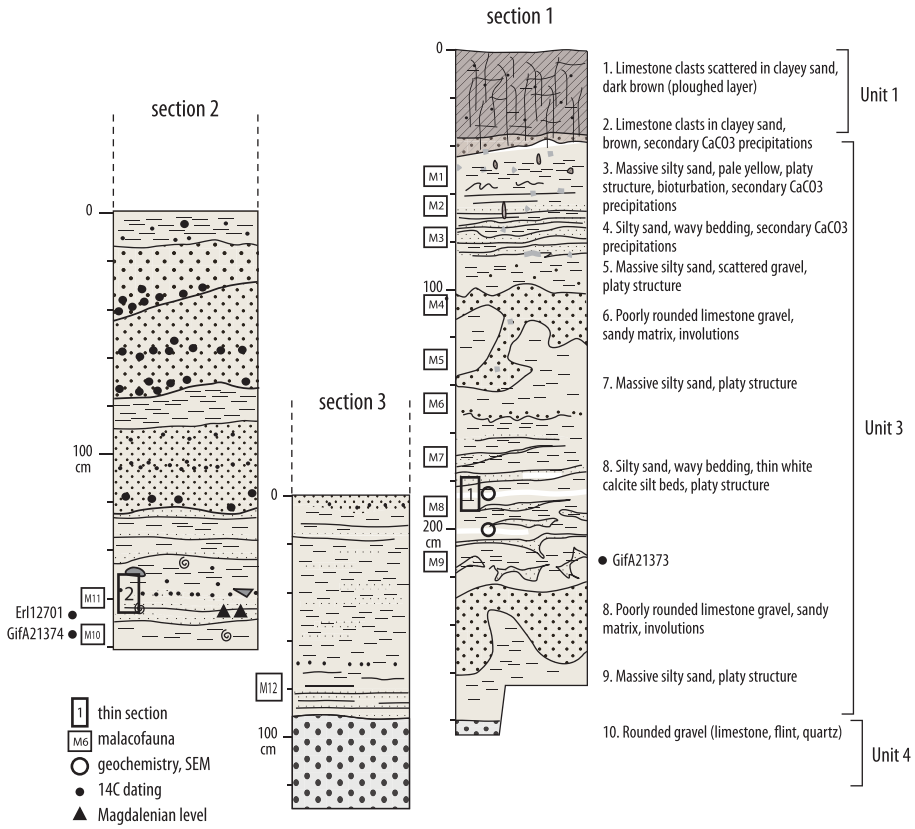

FIGURE 2 Schematic sections in the excavation area and location of the samples for microscopy and malacofauna.

in some silty sand beds, 12 sediment samples of 4 kg each distributed throughout Unit 3 were collected from three sections (Figure 2). The laboratory treatment protocol followed that defined by Puisségur,[23] that is, sieving under water on a 500 µm mesh, gentle drying, and sorting of residues under a binocular microscope.

^{14}C dating was performed at the Laboratoire des Sciences du Climat et de l'Environnement (LSCE) on two gastropod samples, *Trochulus hispidus* (GifA21373) out of the M9 sample in section 1 and *Pupilla muscorum* (GifA21374) out of the M10 sample in section 2. Both samples were cleaned using typical protocol for carbonate ^{14}C dating using HNO_3 0.01 N and transformed into CO_2 on the LSCE semi-automated line.[24] Both samples released sufficient gas to be measured on the solid source of ECHoMICADAS.[25,26] CO_2 graphitization was performed on an automated line (the so-called Gégé line), under pure H_2 in the presence of iron powder as catalyst. Treatment and measurement of samples were done in a series including blanks (IAEA-C1) and international standards (IAEA-C2) to ensure all the process quality. Results are expressed in $F^{14}C$ as recommended by Reimer et al.,[27] and derived ages are reported in BP.[28] Calibration was performed using OxCal software[29] on the IntCal20 calibration curve.[30]

To elucidate the origin of white calcite silt lenses interbedded in the alluvial fan deposits, samples were taken for microscopy, geochemical analyses, and stable isotope analyses ($\delta^{18}O$, $\delta^{13}C$). For samples labeled V1 to V6 (loose powder samples, 66 to 216 µg), the stable isotope ratios were measured using a Micromass MultiPrep device and Optima IRMS at the isotopic facility of EPOC laboratory (University of Bordeaux-CNRS). Acidification of samples was performed at 90°C, and measurements were made by Dual Inlet. Three to six replicates were analyzed for each sample, and the results were averaged. International standard NBS19 was run with the samples. Standard deviations of carbon and oxygen isotope ratios were estimated ±0.04‰ and 0.08‰, respectively, based on standard deviations for all the standards analyzed with the samples.

Thin sections were prepared at PACEA laboratory (University of Bordeaux-CNRS), after sample drying and impregnation under vacuum with a polyester resin. Dry undisturbed samples were also prepared at IRAMAT-CRP2A laboratory, University Bordeaux Montaigne, for scanning electron microscopy (SEM) using a JEOL IT500HR in a low-vacuum mode (40 Pa). One of the white silt beds was subjected to energy dispersive X-ray fluorescence (ED-XRF) analysis using a Bruker Tracer 5i (15 kW, 100 µA, 300 s) and to Raman spectrometry using a Bruker SENTERRA confocal microspectrometer (532 nm at 10 mW, 30*5 s acquisitions with 25*1000 µm slit). As Mg is not detected by ED-XRF, complementary analysis of the Mg/Ca ratio was carried out using SEM coupled with energy-dispersive X-ray spectroscopy (SEM-EDS) with two Oxford Ultimax 100 detectors at 20 kV.

Finally, an undisturbed block of sediment encompassing a white silt bed, a few centimeter-thick, was sent to the Université Savoie Mont Blanc (Le Bourget du Lac) for SEM and X-ray diffractometry (XRD) analyses, and subsamples were analyzed at the University of Newcastle (NSW, Australia, in collaboration with R. Drysdale) for stable isotopes. Some powder samples were analyzed by a scanning electron microscope coupled with an energy dispersive X-ray detector

(SEM–EDX), to visualize the micro-morphology and to identify the chemical composition. A small amount of sample powder was deposited on a carbon conductive adhesive tape stub, then a carbon coating was applied before SEM–EDX analyses by a LEO STEREOSCAN 440 coupled with a X-ray analyzer SDD Bruker in high vacuum mode (beam voltage 10 to 20 keV); images were obtained in secondary electron or backscattering electron modes (platform ASTRE, USMB).

Two powder samples were also prepared from this undisturbed block, specifically from (i) the whitest part of the sample ("white calcite silts") and (ii) the surrounding darker part ("alluvial fan sands"). They were prepared for XXRD analysis (INEL; CoKα X-ray tube; 1.5 × 0.1 slit; reflection mode; generator INEL XRG3D 30 mA, 30 kV; curved position sensitive detector INEL CPS120 for real-time simultaneous data acquisition) to identify the crystalline minerals.

Finally, ~1 mg powder samples were extracted with a dental drill every ~1.5 mm along a profile perpendicular to the bedding in this undisturbed block and sent to the University of Newcastle for oxygen and carbon stable isotope analysis. The powders were digested in 105% orthophosphoric acid at 70°C, and measurements were made using a continuous-flow isotope-ratio mass spectrometer (GV Instruments GV2003). The results were normalized to the Vienna Pee Dee Belemnite (VPDB) scale using internal working standards of Carrara Marble (MAB1—East Kilbride; NEW1—Newcastle), which were cross-checked against the international standards NBS18 and NBS19. Mean analytical precision for both $\delta^{18}O$ and $\delta^{13}C$ is better than 0.1‰.

4 | RESULTS

4.1 | Stratigraphy

The sections observed in the excavation (Figures 2 and 3) show strong variability in the alluvial fan deposits, due to the intercalation of gravel lenses within silty sand units. The coarse sediments are dominant in the northern part where the Magdalenian level has been uncovered and tend to disappear downslope toward the river. The synthetic stratigraphy (Figure 4) includes from base to top:

- A layer of rounded pebbles 3 to 5 cm in diameter (facies Gm,[31]), composed mainly of limestone, flint, and quartz (Figure 3a). This unit (Unit 4) is interpreted as coarse alluvial bar deposits.
- Horizontally bedded pale yellow silty sands (facies SFh), rich in terrestrial molluscan shells and up to 2.5 m thick, with large lenses of poorly rounded limestone gravel (Gh) showing an erosive base (Unit 3, Figure 3b,c). Coarse gravel is dominant upslope and in the upper part of the sequence, where it forms stacked lenses. Laterally, the gravel forms isolated lenses in silty sands. Strong deformations (involutions) are visible as "drops" of gravel material 30 to 40 cm deep descending into finer-grained sediments. In the silty sands, bedding is often wavy and can vanish by place. Beds composed of white calcite silts, a few centimeters thick and up to 2 m wide, are interbedded in the central part of the deposits (Figure 3d). Throughout this unit, a fine platy structure caused by segregation ice lenses[6] is visible (Figure 3e). It is crosscut by a few biogalleries (roots and burrows of the soil fauna). Toward the base, the unit becomes sandier and mottled due to waterlogging. Unit 3 is interpreted as alluvial fan deposits, with possible contributions of overbank alluvium of the Dronne River. The archaeological level is included in this unit at a depth of 3 m (58.1 m a.s.l.).
- Dark grayish brown to greenish brown plastic clays with black ferromanganic spots and polyhedral structure (0.2 to 0.5 m thick, Unit 2). The aggregate surfaces are smooth and shiny (slickensides). This unit, mostly preserved in the downslope part of the excavation, has an irregular lower boundary that corresponds to a decalcification front, locally underlined by a horizon of secondary carbonate precipitation (Bk). These clays are interpreted as a palaeosol (cf. vertic cambisol[32];) developed on the silty sands. Neolithic remains are included in the upper part of the palaeosol.

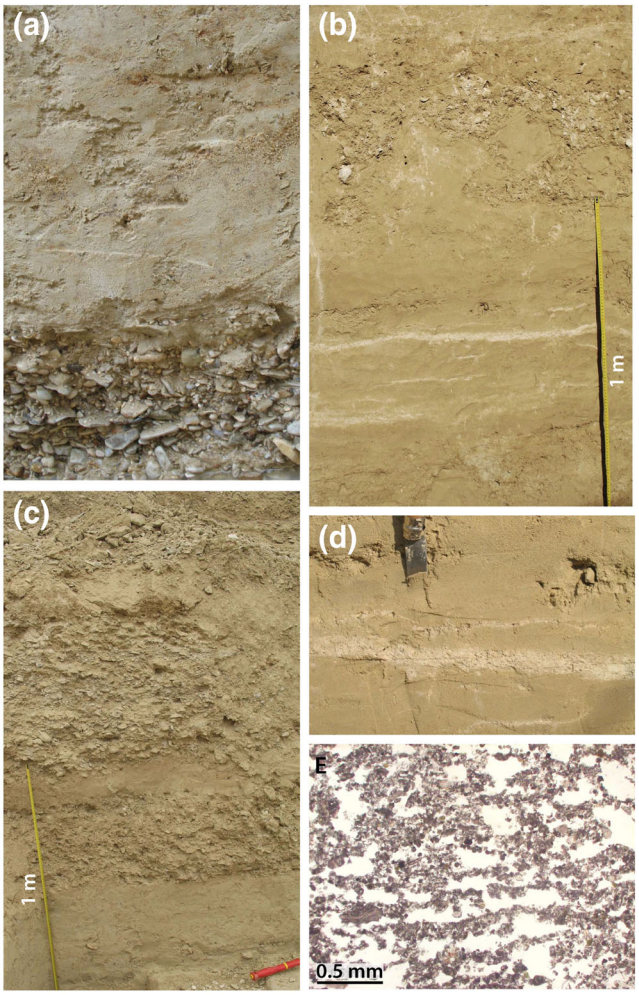

FIGURE 3 View of the main lithofacies. A — Basal gravel layer (Unit 4), the height of the section is 1 m; B — Deformed silty sand and gravel layers (Unit 3); C — Lenses of limestone gravel, upslope part of the alluvial fan (Unit 3); D — Detailed view of a white calcite silt bed; E—Silty sands showing a platy structure, optical microscopy, plain polarized light.

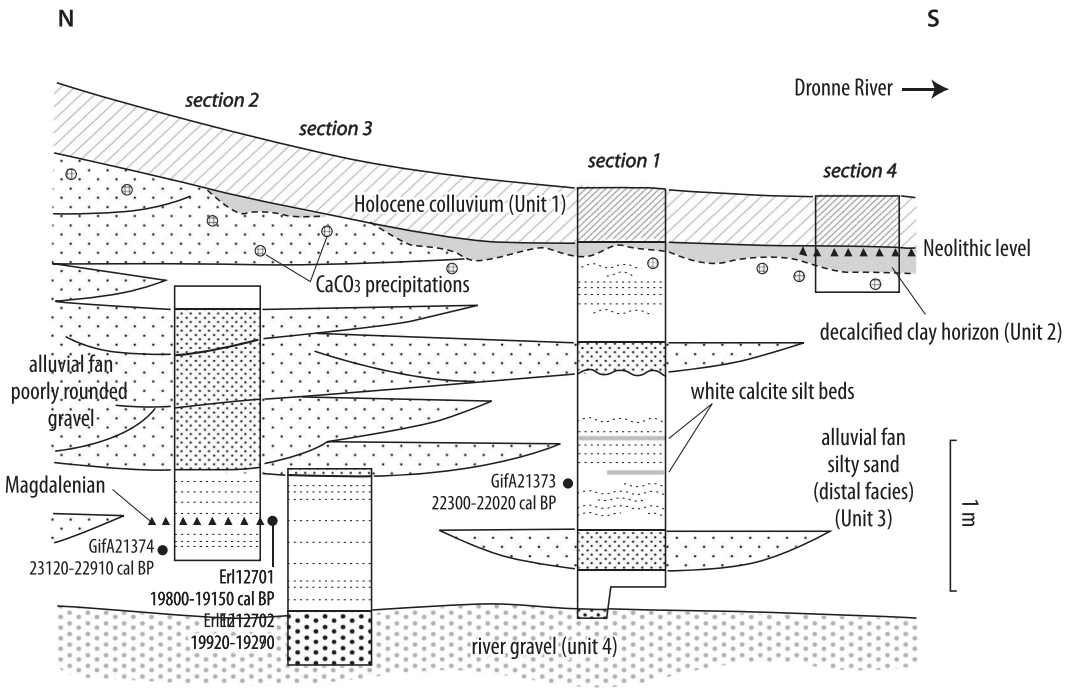

FIGURE 4 Synthetic cross-section of the site. GifA2137-: Radiocarbon age, this study; Erl1270-: Radiocarbon age from Chancerel.[21]

- Dark brown, massive silty clays with abundant scattered limestone gravel, reaching 0.4 to 0.6 m in thickness (Unit 1). They correspond to historical colluvium on which a calcic cambisol has developed.

4.2 | Malacofauna

Most of the deposits yielded few shells, although well preserved (Table 1). According to commonly accepted statistical thresholds,[33] only samples M10 and M11, which bracket the Palaeolithic level (Figure 2), yielded a sufficient quantity of individuals allowing for statistical treatment. The specific distribution shows a predominance of terrestrial taxa. Aquatic molluscs are represented by only two species, of which a few individuals appear in the lower levels (M12 to M9). This distribution indicates the limited influence of aquatic environments.

The terrestrial malacocenosis has a low specific diversity with only seven species. Three are common to almost all levels of Unit 3, *Trochulus hispidus*, *Xerocrassa geyeri*, *P. muscorum*. All are eurythermic taxa; that is, they are resistant to large temperature variations.[34] Among the other taxa sporadically present, *Oxyloma elegans* and *Succinella oblonga* are also frequently recorded in cold climate assemblages but are typical of wet habitats.[23,35] The relative abundance of taxa within the two quantitatively representative assemblages appears unbalanced in favor of *T. hispidus*, which accounts for more than 80% (Figure 5).

This almost-monospecific structure of malacological populations denotes harsh environmental conditions, to which only species with broad ecological valence can adapt. This is the case of *T. hispidus* and *P. muscorum*; the predominance of the former indicates wet conditions specific to lowland environments in contrast to dry steppe areas more favorable to *Pupilla*.[23,36]

4.3 | Chronological data

Two dates were obtained at the Erlangen Radiocarbon Dating Laboratory on charcoal collected from the Palaeolithic level[21] (Figure 4). They, respectively, yielded an age of 16,120 ± 100 BP (Erl-12,701), that is, 19,800–19,150 cal BP (2σ, Intcal20) and 16,250 ± 120 BP (Erl-12,702), that is, 19,920–19,270 cal BP. As both samples come from the same (brief) occupation, a combined age can be calculated that gives 19,820–19,290 cal BP, placing this occupation within the LGM, more specifically in the middle of Greenland Stadial (GS) 2.1.[37]

Two other dates were made at the LSCE of Gif-sur-Yvette on mollusc shells (Table 2). The shells were selected based on their availability and the ecological requirements of species. Indeed, the ingestion of carbon derived from the limestone substratum by molluscs and its incorporation into the shells is a frequent cause of aging (e.g.,[38]). This bias can be limited by selecting small vegetation-dwelling species.[39,40] At Villetoureix, *P. muscorum* and *T. hispidus* were the two taxa that best meet the selection criteria. The age obtained on *P. muscorum* shells from sample M10 located 15 cm below the archaeological level is 19,090 ± 55 BP (GifA21374/ECHo-4,432), that is, 23,122–22,906 cal BP. The second age on *T. hispidus* shells from sample M9 is 18,195 ± 55 BP (GifA21373/ECHo-4,431), that is, 22,304–

TABLE 1 List of mollusc species. *Cecilioides acicula* is a burrowing mollusc whose presence is not contemporaneous with the deposits that contain it, so its numbers are indicated at the end of the table

	Section 3	Section 2		Section 1								
Villetoureix	**M12**	**M10**	**M11**	**M9**	**M8**	**M7**	**M6**	**M5**	**M4**	**M3**	**M2**	**M1**
Oxyloma elegans		3	2				1	1				
Succinella oblonga								2			1	
Vertigo sp.		2										
Pupilla muscorum	6	37	3	2			1	8	2			
Slugs			1									
Trochulus hispidus	6	265	76	9	2	2	2	1		1		1
Xerocrassa geyeri	1	6	1	1		2	1	1	2	1		1
Terrestrial shells	13	313	83	12	2	4	5	13	4	2	1	2
Galba truncatula		1										
Radix labiata	1	5		1								
Aquatic shells	1	6		1								
Total shells	**14**	**319**	**83**	**13**	**2**	**4**	**5**	**13**	**4**	**2**	**1**	**2**
Terrestrial species	3	5	5	3	1	2	4	5	2	2	1	2
Aquatic species	1	2		1								
Total species	**4**	**7**	**5**	**4**	**1**	**2**	**4**	**5**	**2**	**2**	**1**	**2**
Cecilioides acicula											2	2

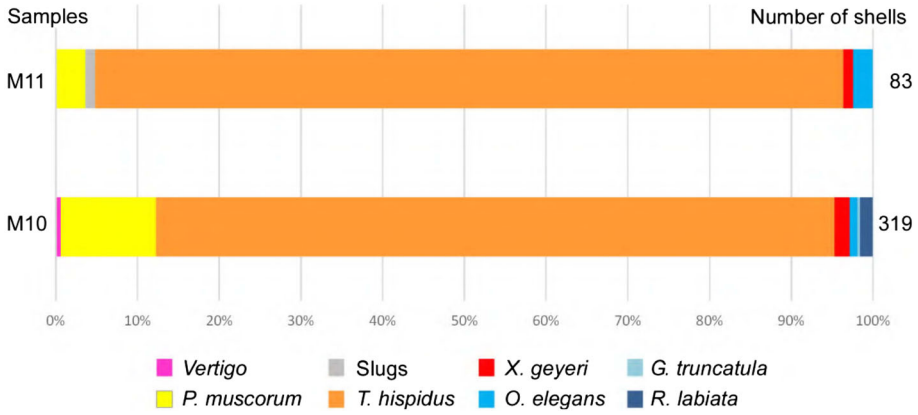

FIGURE 5 Distribution of mollusc species in the two statistically representative samples (M9 and M12).

22,018 cal BP. These ages on shells are slightly older than those obtained on charcoal but remain consistent with GS 2.1.

4.4 | White calcite silts

4.4.1 | Description

Several centimeter-thick beds of white calcite silts appear in the alluvial fan silty sands, particularly in the middle part of the deposits. These calcite silts do not resemble secondary precipitation of pedological origin because of their strata-like appearance, unrelated to soil porosity, and the absence of clearly identifiable macroscopic biological structures. Their association with various evidence of ice formation in the soil (platy structure, involutions) suggests that they developed concurrently with the deposition of silty sand in a periglacial context. At the microscopic scale, they appear as beds composed of small, often aggregated euhedral crystals 3 to 5 μm long covered by a clay matrix in various quantities (Figure 6a). A few tabular sparite crystals up to 600 μm large are also present (Figure 6b). In one sample, root cell pseudomorphs and acicular crystals are observed (Figure 6d). Rounded detrital grains are also visible (Figure 6c). EDX spectra indicate that they are quartz, zircon, and alumino-silicates including biotite. This points to a mixture of different materials, mostly small calcite crystals and detrital grains of alluvial origin. The weak alteration of biotites suggests inputs from the Dronne River as overbank deposition or aeolian inputs rather than by the erosion of old terraces. Secondary carbonates then formed

TABLE 2 Radiocarbon data report of mollusc shells.

Identification				Lab processing[a]			Uncalibrated data[b]			Calibrated age[c,d]		
Sample ID	Sample type	GifA #	ECHo #	Chemistry	Mass [µg C]	Input	F14C	±	Age [BP][e]	±	68.3% probability [range BP]	95.4% probability [range BP]	Median [BP]
Pr1 M9	*Trochulus hispidus*	GifA21373	ECHo-4431	HNO_3 0.01 N	1,380	Gégé - solid source	0.1038	0.0007	18,195	55	22,230 BP–22084 BP	22,304 BP–22018 BP	22,158
Pr2 M10	*Pupilla muscorum*	GifA21374	ECHo-4432	HNO_3 0.01 N	1,260	Gégé - solid source	0.0929	0.0007	19,090	55	23,044 BP–22950 BP	23,122 BP–22906 BP	23,002

[a]Information on chemistry, the conversion mode of the sample to CO_2 and to Cgraphite and the introduction mode in ECHoMICADAS.
[b]Age derives from F14C and is reported following Stuiver and Polach's[28] recommendations, particularly rounding off.
[c]Calibration using online OxCal 4.3 software.[29]
[d]IntCal20: Reimer et al.[30] Radiocarbon. doi: 10.1017/rdc.2020.41.
[e]Rounding off according to Stuiver & Polach,[28] Radiocarbon.

locally in microsites in association with biological activity and gave rise to specific crystal morphologies, that is, root cell pseudomorphs[41,42] and acicular crystals probably corresponding to bioprecipitation by bacteria or fungal hyphae.[41]

4.5 | Geochemical analysis and Raman spectrometry

A white silt bed and its surrounding sediments were analyzed using ED-XRF. Compared to the alluvial silty sands, the white bed is significantly richer in calcium (Ca) and poorer in elements associated with alumino-silicates (Si, Al, K, Rb) and oxides (Fe, Mn, Ti) (Figure S1). SEM-EDS analysis shows that the Mg/Ca ratio is lower in the white silt bed compared to alluvial detrital calcite (Table 3). Raman spectroscopy and XRD confirm the calcite composition of the white silts, with rare detrital grains identified as quartz and plagioclase (Figure S2). It confirms as well that the calcite in the alluvial silty sands and in the white silts does not have the same crystalline properties, the latter being better crystallized.

4.6 | Isotopic analyses

Various types of carbonates were sampled for isotopic analyses (Figure 7; Table 4). These are (i) fragments of Campanian (marine) limestone, (ii) alluvial fan silty sand, (iii) secondary carbonates of biological origin, either loose (pseudomycelium) or indurated (calcite pendants on gravels) from the Bk horizon of the Holocene soil, and (iv) calcite silts forming the white beds.

The obtained values highlight three types of material (Figure 7a). Limestone samples and alluvial sands display similar values, ranging from −1 to −2‰ for $\delta^{18}O$ and close to 2‰ for $\delta^{13}C$, which is expected for marine limestone. Carbonates of biological origin (bioprecipitation) are characterized by significant depletion in heavy isotopes (−4 to −5‰ for $\delta^{18}O$, −5 to −9‰ for $\delta^{13}C$), whereas the white silt beds show intermediate values. These samples form a separate group on the $\delta^{13}C$ versus $\delta^{18}O$ diagram and plot close to a straight line. Measurements made on the undisturbed sample along a profile perpendicular to a white silt bed show strong covariance between $\delta^{13}C$ and $\delta^{18}O$ ($R^2 = 0.9574$) and confirm the difference in isotopic composition between the white silts, at the center of the profile presented here, and the alluvial silty sands on either side (Figure 7b).

5 | DISCUSSION

5.1 | Sedimentary sequence

The sections show four main pedo-sedimentary units. The oldest unit (Unit 4) corresponds to a gravel body, whose altitude shows that it is an integral part of the basal coarse-grained floodplain alluvium. The

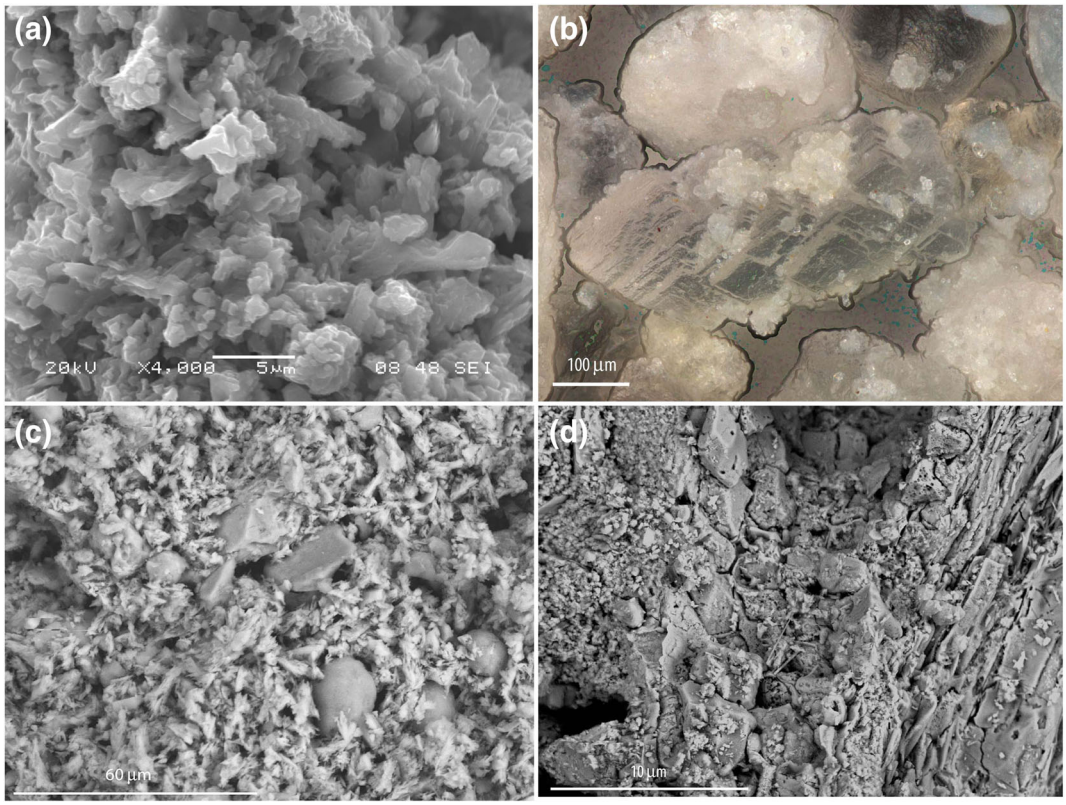

FIGURE 6 Microscopic view of a white calcite silt bed. A — Aggregated small calcite crystals (scanning electron microscopy [SEM]); B — Large plate-like calcite crystal partly covered with small crystals (optical microscopy); C — Clayey calcite silt and detrital sand grains (SEM); D — Calcite pseudomorhs after root cells; a few acicular crystal are also visible (SEM).

TABLE 3 Mg/Ca ratio of various samples from detrital calcite and white calcite silts.

Sediment type	Spectrum number	Mg (%)	Ca (%)	Mg/Ca	Mean	Standard dev.
Alluvial silty sand zone 1	1	1.54	43.92	0.0351	0.0360	0.0017
Alluvial silty sand zone 1	2	1.55	39.68	0.0391		
Alluvial silty sand zone 1	3	1.49	42.88	0.0347		
Alluvial silty sand zone 1	4	1.55	45.99	0.0337		
Alluvial silty sand zone 2	5	1.52	40.31	0.0377		
Alluvial silty sand zone 2	6	1.56	42.44	0.0368		
Alluvial silty sand zone 2	7	1.47	40.8	0.0360		
Alluvial silty sand zone 2	8	1.5	42.68	0.0351		
Cryogenique calcite zone 3	9	1.18	56.95	0.0207	0.0166	0.0029
Cryogenique calcite zone 3	10	1.13	59.86	0.0189		
Cryogenique calcite zone 3	11	0.91	67.26	0.0135		
Cryogenique calcite zone 3	12	0.8	66.48	0.0120		
Cryogenique calcite zone 4	13	1.04	62.9	0.0165		
Cryogenique calcite zone 4	14	0.95	62.09	0.0153		
Cryogenique calcite zone 4	15	1.08	59.46	0.0182		
Cryogenique calcite zone 4	16	1.03	58.75	0.0175		

ages obtained on the overlying deposits imply that the gravel emplacement predates ca. 23 ka and was deposited by the river during the Last Glacial.

Unit 3 corresponds to alluvial fan deposits, mainly fed by the erosion of Campanian limestone. The torrential dynamics was favored during the LGM by strong production of debris due to frost

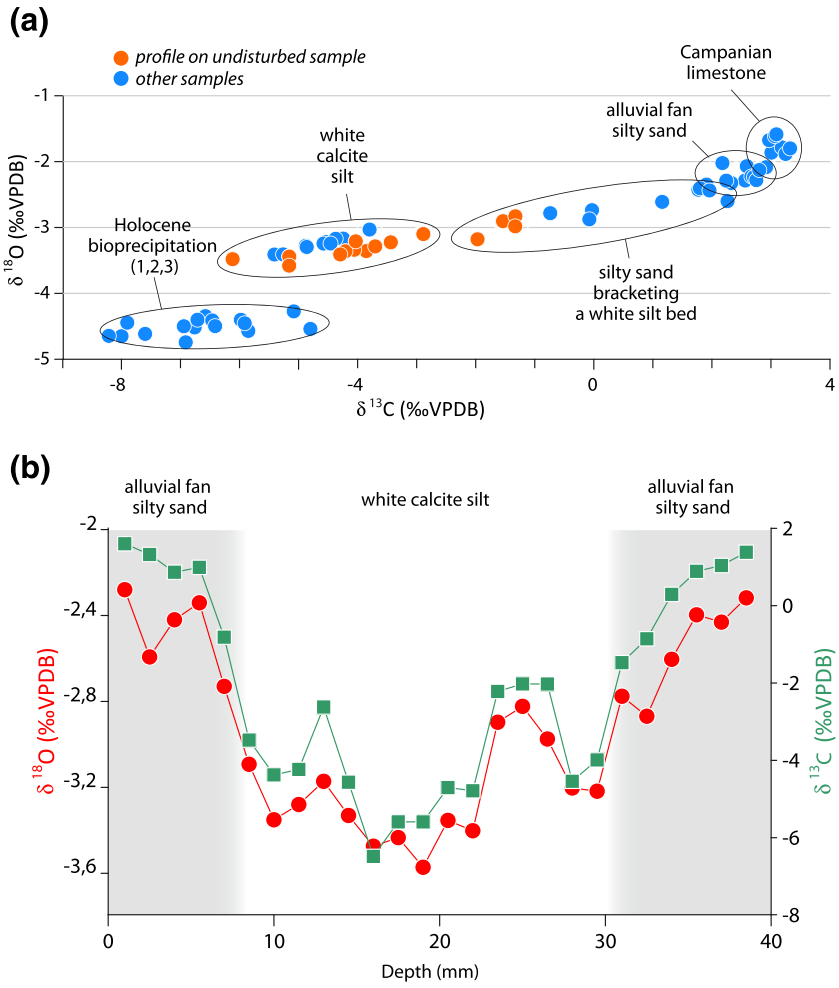

FIGURE 7 Isotopic analyses. A — Isotope composition of various carbonate types. B — Profile of isotope composition through a 4-cm-thick sample composed of a bed of white calcite silt bracketed by alluvial fan silty sand.

weathering of the limestone, by sparse vegetation, and probably, by seasonal ground sealing by frost (e.g.,[43,44]). The stacked gravel lenses in the upper part, which correspond to the coarse load deposited in ephemeral channels crossing the alluvial fan, reflect the downstream progradation of proximal facies over time, in conjunction with progressive fan extension. The distal silty sand facies were strongly affected by periglacial phenomena, in particular the formation of segregation ice lenses and involutions. Within the regional context, where the presence of permafrost during the LGM is unlikely,[1,3] these phenomena developed in relation to deep seasonal frost.

A soil then developed on the fan deposits (Unit 2) and led to their decalcification. Because of the clayey texture and poor drainage, the soil shows hydromorphic (mottling) and vertic properties (slickensides related to alternating shrinkage and swelling of the clays, dark color due to deep incorporation of organic matter). It reflects the cessation of alluvial fan deposition during the Holocene and concomitant alteration by soil-forming processes. This soil was later partially eroded and buried by coarser-grained sediments, interpreted as agricultural colluvium (Unit 1). The coarse fraction derives from the erosion and redistribution by agricultural tools of older gravelly sediments and/or from sporadic torrential inputs mixed with the soil by ploughing.

5.2 | Palaeoenvironmental data derived from the malacofauna

The composition of the malacofauna of Villetoureix is similar to that known for cold period assemblages in France,[23,35,45] which are characterized by low diversity and species with a wide ecological range able to adapt to contrasting temperatures. The strong predominance of *T. hispidus* over the other species indicates harsh climatic conditions. This imbalance in favor of a single taxon has already been observed in northern France during the first half of the Younger Dryas.[46]

All the species collected at Villetoureix are still known today in the region except for *Xerocrassa geyeri*. This taxon, typical of dry and open habitats with little vegetation, was not found during the last census of malacofaunas carried out in the Dordogne district, southwest France.[47] Its modern distribution is mostly central European but also includes highland stations in southeastern France and Spain.[34] In Burgundy (eastern France), *X. geyeri* is typical of Pleistocene assemblages of transitional phases between cold and temperate periods.[23] The species is also regularly recorded during the Allerød in northern France.[48,49]

In southwest France, *X. geyeri* has been recorded from Weichselian loess sequences near Toulouse.[50] The malacological

TABLE 4 Stable isotope composition of samples.

Sample ref.	δ13C (‰VPDB)	δ18O (‰VPDB)	Nature	Laboratory	Depth (mm)
V1	−5.34	−3.28	White silts 1	EPOC	
V1	−5.02	−3.22		EPOC	
V1	−4.75	−3.17		EPOC	
V1	−5.06	−3.24		EPOC	
V1	−5.32	−3.30		EPOC	
V2	−4.87	−3.17	White silts 2	EPOC	
V2	−4.95	−3.24		EPOC	
V2	−5.83	−3.41		EPOC	
V2	−5.70	−3.41		EPOC	
V2	−4.33	−3.03		EPOC	
Vil 06-09	−3.48	−3.10	White silts 3	NSW	*8.5*
Vil 07-09	−4.38	−3.36		NSW	*10*
Vil 08-09	−4.24	−3.29		NSW	*11.5*
Vil 09-09	−2.63	−3.18		NSW	*13*
Vil 10-09	−4.57	−3.34		NSW	*14.5*
Vil 11-09	−6.49	−3.48		NSW	*16*
Vil 12-09	−5.60	−3.44		NSW	*17.5*
Vil 13-09	−5.60	−3.58		NSW	*19*
Vil 14-09	−4.71	−3.36		NSW	*20.5*
Vil 15-09	−4.79	−3.41		NSW	*22*
Vil 16-09	−2.23	−2.90		NSW	*23.5*
Vil 17-09	−2.03	−2.83		NSW	*25*
Vil 18-09	−2.03	−2.98		NSW	*26.5*
Vil 19-09	−4.55	−3.21		NSW	*28*
Vil 20-09	−4.00	−3.23		NSW	*29.5*
Vil 01-09	1.59	−2.29	Margin of white silt bed	NSW	*1*
Vil 02-09	1.32	−2.60		NSW	*2.5*
Vil 03-09	0.86	−2.43		NSW	*4*
Vil 04-09	0.98	−2.35		NSW	*5.5*
Vil 05-09	−0.82	−2.74		NSW	*7*
Vil 21-09	−1.48	−2.78		NSW	*31*
Vil 22-09	−0.86	−2.88		NSW	*32.5*
Vil 23-09	0.29	−2.61		NSW	*34*
Vil 24-09	0.88	−2.40		NSW	*35.5*
Vil 25-09	1.03	−2.44		NSW	*37*
Vil 26-09	1.37	−2.33		NSW	*38.5*
V1	1.62	−2.07	Alluvial fan sand	EPOC	
V1	1.69	−2.23		EPOC	
V1	1.92	−2.09		EPOC	
V1	1.30	−2.29		EPOC	
V1	1.24	−2.02		EPOC	
V2-A	−7.09	−4.52	Bioprecipitation 1	EPOC	
V2-A	−6.92	−4.35		EPOC	
V2-A	−7.05	−4.40		EPOC	
V2-A	−6.81	−4.41		EPOC	
V2-A	−7.26	−4.50		EPOC	

TABLE 4 (Continued)

Sample ref.	δ13C (‰VPDB)	δ18O (‰VPDB)	Nature	Laboratory	Depth (mm)
V2-B	−6.24	−4.57	Bioprecipitation 2	EPOC	
V2-B	−6.77	−4.50		EPOC	
V2-B	−6.36	−4.40		EPOC	
V2-B	−5.26	−4.54		EPOC	
V2-B	−6.30	−4.45		EPOC	
V2-B	−5.53	−4.27		EPOC	
V4	−7.23	−4.74	Bioprecipitation 3	EPOC	
V4	−8.24	−4.65		EPOC	
V4	−7.87	−4.62		EPOC	
V4	−8.44	−4.65		EPOC	
V4	−8.15	−4.45		EPOC	
V5	2.01	−1.86	Campanian limestone 1	EPOC	
V5	2.17	−1.78		EPOC	
V5	2.23	−1.88		EPOC	
V5	2.30	−1.80		EPOC	
V6-A	1.97	−1.68	Campanian limestone 2	EPOC	
V6-A	2.06	−1.61		EPOC	
V6-A	2.09	−1.59		EPOC	
V6-B	1.73	−2.24	Campanian limestone 3	EPOC	
V6-B	1.77	−2.28		EPOC	
V6-B	1.82	−2.13		EPOC	

Note: Laboratory codes: EPOC—Université de Bordeaux-CNRS; NSW—University of Newcastle.
Abbreviation: VPDB, Vienna Pee Dee Belemnite.

study carried out on Lateglacial alluvial deposits at Bergerac[51] has suggested that the development of this taxon in Dordogne as early as the Bølling resulted from the greater proximity of refuge areas compared to northern regions. Its occurrence at Villetoureix, in small but constant numbers, confirms its presence in the lowlands of southern France during the LGM. Similarly, *X. geyeri* retreated to highland stations in Provence (southeastern France) during the warm periods and colonized the lowlands during the cold phases of the Last Glacial, where it is considered a marker of worsening climatic conditions.[52]

Overall, the environmental and climatic signal provided by the malacofauna of Villetoureix is unequivocal and indicates an open environment, with little vegetation and cold climatic conditions.

5.3 | White calcite silts

The thin, a few meters wide, white calcite silt lenses interbedded in the middle part of the alluvial sequence are unusual features. Several arguments clearly demonstrate that they do not correspond to secondary precipitations of pedological origin. The arguments include (i) the strata-like pattern; (ii) the general lack of calcified plant, bacterial, or fungal features (apart from a few very localized bioprecipitation associated with root traces); (iii) their isotopic composition, which is significantly different from that of Holocene biogenic carbonates; and (iv) evidence for synsedimentary deposition. Their isotopic composition also indicates that they do not originate from the breakdown of Campanian limestone.

Given the depositional context (distal part of an alluvial fan, periglacial environment), an origin in connection with the formation of ice bodies, that is, icings (aufeis) or open-system frost blisters can be envisaged. Icings are seasonal ice layers that form on the ground in cold environments (permafrost or deep seasonal frost context) at the emergences of groundwater when subsurface circulations are made impossible due to soil sealing by frost.[53–57] Karst regions where subsurface flows predominate are particularly favorable for their development.[53] Icings can also be fed by rivers, when water locally breaks through the superficial ice layer and flows onto the plain.[53,58] Such ice accumulations can reach up to 2 m in thickness. Open-system frost blisters are small mounds that form when the increase in interstitial water pressure causes hydraulic fracturing of the ground and uplift of the frozen top layer due to continuous water supply, often in spring outflow channels (e.g.,[57,59]). Freezing of the water lenses generates intrusive ice layers of varying thickness and extent.

Water freezing causes precipitation of dissolved carbonates.[9,60] In the icings described by Lacelle[9] from permafrost areas of arctic Canada, water circulation and precipitation of fine-grained calcite occur primarily under the ice, in contact with the ground. During thawing, cryogenic calcite concentrates in melt channels and is

deposited in patches on the ground. Hall,[54] for instance, described loose calcite accumulations locally reaching 1–10 cm thick after icing melt in Alaska. SEM images of the calcite crystals show various morphologies. In the Yukon examples analyzed by Lacelle,[9] the calcite crystals have essentially a rod-like morphology up to 150 μm long and less than 10 μm wide, while Bukowska-Jania[61] described flattened aggregates of 1–100 μm crystals in icings from Svalbard. In contrast, the Villetoureix samples comprise mainly aggregates of small crystals less than 5 μm long (Figure 6). It can be envisaged that crystal redistribution by meltwater and diagenesis (compaction, dissolution-precipitation) has somewhat influenced their morphology. However, the absence of residual rod morphologies lends support to the hypothesis of original calcite precipitation as small chunky crystals. Their small size is probably related to a short-lived precipitation.

Various studies on modern icings have also focused on the isotopic composition of cryogenic calcite.[9,56,62,63] It has been shown that this composition is typified by specific values, different from those found in other types of calcite precipitates, especially those controlled by biological activity. It depends mainly on the composition of the water from which the calcite precipitated, its saturation with respect to calcite, the kinetic fractionation during precipitation and the freezing rate.[63] When compared with the values of icing calcites analyzed by the authors cited earlier, the Villetoureix $\delta^{13}C$ values are within a comparable range, while the $\delta^{18}O$ is much higher (from −2.8 to −3.5‰ VPDB vs. − 18 to −37‰ VPDB; e.g.,[63]). Indeed, the very negative values of modern icing calcite are largely due to the latitudinal difference (i.e., the isotopic composition of parent water depends on the isotopic composition of meteoric waters, which is influenced by air temperature and distance to the moisture source[64]). Instead, the calcite $\delta^{13}C$ reflects the $\delta^{13}C$ of the dissolved inorganic carbon of the parent water and the conditions of isotopic fractionation occurring during crystallization.

The range of $\delta^{18}O$ and $\delta^{13}C$ values of the white silt beds from Villetoureix is rather narrow, and the values do not evolve in the opposite direction as in cryogenic calcite formed in open-system environment, like cryogenic cave carbonates[14] and some examples of cryogenic calcite from icings.[65] In the context of an alluvial fan, we must assume that some admixture occurred between the white calcite silts and the surrounding detrital carbonates, which could explain part of the isotopic range and, particularly, the apparent covariation of $\delta^{13}C$ and $\delta^{18}O$ values, which stretch between the two poles of data (Figure 7).

Nevertheless, the isotopic values of Villetoureix calcite silts share their characteristics with cryogenic calcite described in icings formed in areas with limestone bedrock and where precipitation occurred in a closed system. In such environments, water is at or near saturation with respect to calcite, and calcite can readily precipitate under equilibrium conditions during the initial stage of freezing.[9,63] Water freezing in a closed system results in the progressive depletion in ^{18}O of the residual water (due to preferential incorporation of heavy isotopes in the ice). It also maintains CO_2 in solution resulting in some isotopic equilibration with HCO_3^- and prevents exchanges with the atmosphere, both keeping low values of $\delta^{13}C_{DIC}$.[63] This is consistent with the observed isotopic values for the white silts of Villetoureix. In contrast, open-system precipitation causes severe ^{13}C enrichment of the calcite as a result of CO_2 degassing and preferential escape of light CO_2 to the atmosphere. These would draw $\delta^{13}C$ to very high values, which is not the case at Villetoureix. Alternatively, near-equilibrium precipitation could have occurred in frost blisters. Intrusive ice lenses in the ground, fed by continuous underground water supply (e.g.,[57,59]), may allow similar calcite precipitation under closed-system conditions. The melting of ice lenses may be involved in the later formation of involutions in the overlying sediments (e.g.,[66]).

As a test for our hypothesis, we evaluated the isotopic composition of a calcite that would have formed in equilibrium from local groundwater during the LGM. We used the data from Saltel et al.[2] who have provided isotopic composition of groundwater in regional aquifers for the Last Glacial. In particular, three water samples have a dead-carbon corrected radiocarbon age close to that of the cryogenic calcite at Villetoureix (Table 5). We used their isotopic composition to calculate the theoretical isotopic composition of calcite that would have precipitated from this water, at a temperature of 0°C. Based on Kim and O'Neil[67] equation, we obtained mean $\delta^{18}O_{calcite}$ values close to those measured in Villetoureix calcite, which strongly suggests that precipitation occurred close to the freezing point. We also determined the temperature interval required to obtain the observed range of $\delta^{18}O$ of Villetoureix calcite using the different aquifer $\delta^{18}O$ values. The temperature appears to have been close to 0°C. Positive temperature can be excluded in this context, which highlights some uncertainties in the data. Two main sources of uncertainties can be evoked: (i) the aquifer $\delta^{18}O$ values are not representative of the water at the origin of calcite deposition during the LGM at Villetoureix (this is obviously the case for sample 08257-0073 from the Oligocene aquifer) and (ii) the Villetoureix calcite samples yielding slightly negative $\delta^{18}O$ values (i.e., between ∼ − 2 to −3‰) do not correspond to pure cryogenic calcite but, as mentioned earlier, to a mixture between cryogenic and detrital calcite. It is particularly likely for samples taken from the margins of the white silt beds, whose $\delta^{18}O$ values plot closer to the pole of detrital carbonates.

As reported by Zak et al.,[14] cryogenic calcite is also characterized by a lower Mg/Ca ratio than other calcite types precipitated from the same parent water due to better incorporation of Mg ions into the ice than larger Ca ions. This is consistent with the significantly lower ratio found by SEM-EDS analysis in white calcite silts than in alluvial detrital calcite, assuming that the Mg/Ca ratio of the groundwater was close to that of the host limestone.

In conclusion, contextual, morphological, and isotopic evidence converges to propose that this fine-grained calcite, whose accumulation is at the origin of the thin white beds intercalated in the alluvial fan, is of cryogenic origin. Isotopic evidence indicates that calcite precipitation occurred under closed-system conditions in connection with freezing of mineralized water. In the geomorphological context of Villetoureix associated with deep seasonal ground freezing, it is likely that during the LGM, icings and possibly, thick intrusive ice lenses (frost blisters) formed periodically on the lower slopes of the alluvial fan due to continuous water supply from the karst (Figure 8). Seasonal

TABLE 5 Calculated equilibrium isotopic composition of cryogenic calcite at Villetoureix using the Last Glacial Maximum isotopic composition of regional aquifers from Saltel et al.[2]

Sample No	Mean age (cal ka BP)	δ18O (‰ VSMOW)	Aquifer	Calculated δ18Oc for a hypothetical T° = 0 °C	Observed range or δ18Oc in Villetoureix calcite silts	Calculated T° for the observed range of δ18Oc
08257-0073	19 ± 1	−6.11	Oligocene	−2.72	−2.83 to −3.58	+0.3 to +3.7
08272-0136	23.4 ± 0.8	−6.49	Campanian	−3.10		−1.3 to +2.0
08525-0028	21.2 ± 0.6	−6.90	Oligocene	−3.51		−3.0 to +0.3

Note: VSMOW, Vienna Standard Mean Ocean Water.

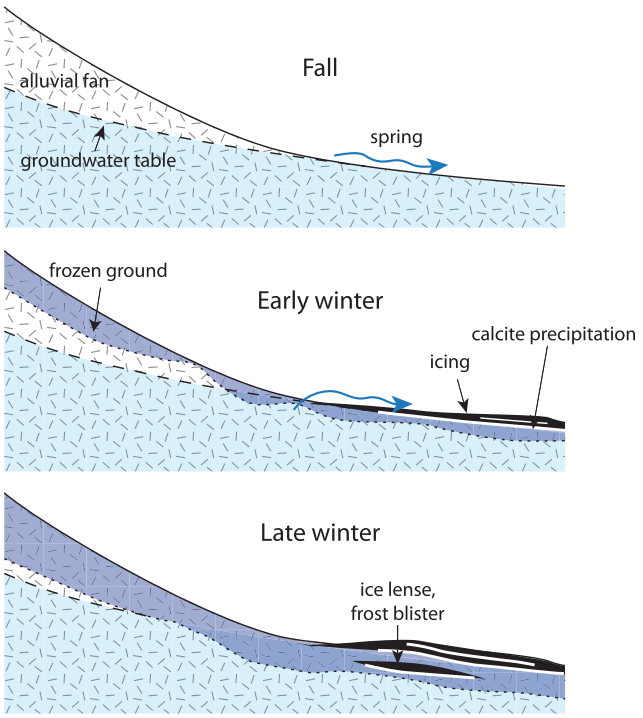

FIGURE 8 Probable formation processes of the beds of cryogenic calcite at Villetoureix.

freezing was associated with the precipitation of small calcite crystals trapped in the ice. As the ice melted, the calcite powder was more or less remobilized and mixed with detrital inputs.

6 | CONCLUSION

The study site is located on an alluvial fan at the mouth of a dry valley tributary of the Dronne River and spreading over the alluvial plain. At the time of the prehistoric occupation, which occurred during the LGM, the torrential dynamics was favored by strong production of debris due to frost weathering of the limestone outcrops, by sparse vegetation, and by seasonal sealing of the ground by frost. Abundant traces of ice formation in the sediments, including platy structure and involutions, suggest a deep seasonal frost context. The lenses of white calcite silts interbedded in the alluvial fan silty sands show specific chemical composition, crystal morphology, and most of all, an isotopic signature consistent with fine-grained cryogenic calcite formed under closed-system conditions. Therefore, they are interpreted as evidence of calcite precipitation caused by the seasonal freezing of groundwater of karstic origin (close to saturation with respect to calcite), leading to the formation of icings and/or frost blisters at the foot of the slope. This type of calcite deposit was never before described in Pleistocene deposits in France. Nevertheless, it must have been relatively common during the glacial periods in the calcareous regions of southwest France.

ACKNOWLEDGMENTS

We warmly thank J.P. Chadelle and A. Michel (Service Départemental de l'Archéologie de la Dordogne) who asked us to participate in the study of the site, R. Drysdale (University of Newcastle, Australia) for having carried out part of the isotope analyses, O. Romeyer and E. Chalmin (Université Savoie Mont Blanc) for SEM and XRD analyses, respectively (plateforme ASTRE, USMB). We also acknowledge three anonymous reviewers for their constructive comments. Funding was provided by the Institut National de Recherches en Archéologie Préventive and the Service Départemental de l'Archéologie de la Dordogne.

DATA AVAILABILITY STATEMENT

The data that support the findings of this study are available from the corresponding author upon reasonable request.

ORCID

Pascal Bertran https://orcid.org/0000-0003-3334-9869
Isabelle Couchoud https://orcid.org/0000-0002-7166-9575

REFERENCES

1. Andrieux E, Bertran P, Saito K. Spatial analysis of the French Pleistocene permafrost by a GIS database. *Permafrost and Periglacial Processes*. 2016;27(1):17-30. doi:10.1002/ppp.1856
2. Saltel M, Rebeix R, Bertrand T, Francesci M, Lavielle B, Bertran P. Paleoclimate variations and impact on groundwater recharge in multilayer aquifer systems using a multi-tracer approach (northern Aquitaine basin – France). *Hydrgeol J*. 2019;27(4):1439-1457. doi:10.1007/s10040-019-01944-x
3. Stadelmaier KH, Ludwig P, Bertran P, et al. A new perspective of permafrost boundaries in France during the last glacial maximum. *Climate of the Past*. 2021;17(6):2559-2576. doi:10.5194/cp-17-2559-2021
4. Andrieux E, Bateman M, Bertran P. The chronology of Late Pleistocene thermal contraction cracking derived from sand wedge dating in

central and southern France. *Global Planetary Change*. 2018;162:84-100. doi:10.1016/j.gloplacha.2018.01.012
5. Bertran P, Andrieux E, Antoine P, Deschodt L, Font M, Sicilia D. Pleistocene involutions and patterned ground in France: examples and analysis using a GIS database. *Permafrost and Periglacial Processes*. 2017;28(4):710-725. doi:10.1002/ppp.1957
6. Van Vliet-Lanoë B. Frost action. In: Stoops G, Marcelino V, Mees F, eds. *Interpretation of micromorphological features of soils and Regoliths*. Amsterdam: Elsevier; 2010:81-108. doi:10.1016/B978-0-444-53156-8.00006-4
7. Kervazo B, Texier JP. Le site paléolithique de la Grotte XVI (Dordogne, France): lithostratigraphie, processus de formation et essaie de chronologie. *Paleo*. 2011;21(21):163-188. doi:10.4000/paleo.1805
8. Texier JP. Nouvelle lecture géologique du site paléolithique du Pech-de-l'Azé II (Dordogne, France). *Paleo*. 2006;18:217-236.
9. Lacelle D. Environmental setting, (micro)morphologies and stable C-O isotope composition of cold climate carbonate precipitates – a review and evaluation of their potential as paleoclimatic proxies. *Quaternary Science Reviews*. 2007;26(11-12):1670-1689. doi:10.1016/j.quascirev.2007.03.011
10. Zák K, Onac BP, Persoiu A. Cryogenic carbonates in cave environments: a review. *Quat Int*. 2008;187(1):84-96. doi:10.1016/j.quaint.2007.02.022
11. Zák K, Richter DK, Filippi M, et al. Coarsely crystalline cryogenic cave carbonate - a new archive to estimate the last glacial minimum permafrost depth in Central Europe. *Climate of the Past*. 2012;8(6):1821-1837. doi:10.5194/cp-8-1821-2012
12. Courty MA, Marlin C, Dever L, Tremblay P, Vachier P. The properties, genesis and environmental significance of calcitic pendents from the high Arctic (Spitzbergen). *Geoderma*. 1994;61(1-2):71-102. doi:10.1016/0016-7061(94)90012-4
13. Thiry M, Innocent C, Girard JP, Milnes AR, Franke C, Guillon S. Sand calcites as a key to Pleistocene periglacial landscapes. *Quatern Res*. 2021;101:225-244. doi:10.1017/qua.2020.98
14. Zák K, Onac BP, Kedebskaya OI, Filippi M, Dublyansky Y, Luestcher M. Cryogenic mineral formation in caves. In: Perşoiu A, Lauritzen SE, eds. *Ice caves*. Elsevier; 2018:123-162. doi:10.1016/B978-0-12-811739-2.00035-8
15. Bartolomé M, Sancho C, Osácar MC, et al. Characteristics of cryogenic carbonates in a Pyrenean ice cave (northern Spain). *Geogaceta*. 2015;58:107-110.
16. Richter DK, Meissner P, Immenhauser A, Schulte U, Dorsten I. Cryogenic and non-cryogenic pool calcites indicating permafrost and non-permafrost periods: a case study from the Herbstlabyrinth-advent cave system (Germany). *The Cryosphere*. 2010;4(4):501-509. doi:10.5194/tc-4-501-2010
17. Zák K, Urban J, Cilek V, Hercman H. Cryogenic cave calcite from several central European caves: age, carbon and oxygen isotopes and a genetic model. *Chem Geol*. 2004;206(1-2):119-136. doi:10.1016/j.chemgeo.2004.01.012
18. Sharp M, Tison JL, Fierens G. Geochemistry of subglacial calcite: implications for the hydrology of the basal water film. *Arctic and Alpine Research*. 1990;22(2):141-152. doi:10.2307/1551299
19. Lipar M, Martín-Pérez A, Tičar J, et al. Subglacial carbonate deposits as a potential proxy for a glacier's former presence. *The Cryosphere*. 2021;15(1):17-30. doi:10.5194/tc-15-17-2021
20. Bourbon P. *Gestion des eaux souterraines en Région Aquitaine. Carte géologique numérique à 1/250 000 de la région Aquitaine*; 2019. Notice technique. Rapport final, BRGM/RP-68881-FR.
21. Chancerel G. *Villetoureix (Dordogne)*. Rapport de diagnostic archéologique, Conseil Général de la Dordogne, Périgueux, 103 p; 2007. doi:10.4000/adlfi.7838
22. Chadelle JP. *Etude préliminaire du secteur magdalénien*Rapport de fouille archéologique, Conseil Général de la Dordogne, Périgueux. Vol. 5; 2009. 65 p.
23. Puisségur JJ. *Mollusques continentaux quaternaires de Bourgogne*. Doin, Paris: Mémoires Géologiques de l'Université de Dijon n°3; 1976. 241 p.
24. Tisnérat-Laborde N, Poupeau J-J, Tannau J-F, Paterne M. Development of a semi-automated system for routine preparation of carbonate samples. *Radiocarbon*. 2001;43(2A):299-304. doi:10.1017/S0033822200038145
25. Synal HA, Stocker M, Suter M. MICADAS: a new compact radiocarbon AMS system. *Nuclear Instruments & Methods in Physics Research, Section B-Beam Interactions with Materials and Atoms*. 2007;259(1):7-13. doi:10.1016/j.nimb.2007.01.138
26. Tisnérat-Laborde N, Thil F, Synal H-A, et al. ECHoMICADAS: a new compact AMS system to measuring 14C for environment, *climate and human sciences*. In: *22nd international radiocarbon conference, Dakar, Senegal, 16-20 November 2015*; 2015. PHYS-O.05.
27. Reimer PJ, Brown TA, Reimer RW. Discussion; reporting and calibration of post-bomb 14C data. *Radiocarbon*. 2004;46:1299-1304.
28. Stuiver M, Polach HA. Discussion: reporting of 14C data. *Radiocarbon*. 1977;19(3):355-363. doi:10.1017/S0033822200003672
29. Bronk RC. Bayesian analysis of radiocarbon dates. *Radiocarbon*. 2009;51(1):337-360.
30. Reimer PJ, Austin WEN, Bard E, et al. The IntCal20 northern hemisphere radiocarbon age calibration curve (0–55 cal kBP). *Radiocarbon*. 2020;62(4):725-757. doi:10.1017/rdc.2020.41
31. Miall AD. *The geology of fluvial deposits. Sedimentary facies, basin analysis, and petroleum geology*. Berlin: Springer; 1996. 582 p.
32. WRB. World Reference Base for Soil Resources, IUSS Working Group. In: *World soil resources reports 103*. 2nd ed. Rome: FAO; 2006.
33. Evans J. *Land snails in archaeology*. London: Seminar Press; 1972. 436 p.
34. Welter-Schultes FW. *European non-marine molluscs, a guide for species identification*. Göttingen: Planet Poster Editions; 2012. 674 p.
35. Moine O. West-European malacofauna from loess deposits of the Weichselian upper Pleniglacial: compilation and preliminary analysis of the database. *Quaternaire*. 2008;19(1):11-29.
36. Limondin-Lozouet N, Gauthier A. Biocénoses pléistocènes des séquences loessiques de Villiers-Adam (Val d'Oise, France): études malacologiques et palynologiques. *Quaternaire*. 2003;14(4):237-252. doi:10.3406/quate.2003.1745
37. Rasmussen SO, Bigler M, Blockley SP, et al. A stratigraphic framework for abrupt climatic changes during the last glacial period based on three synchronized Greenland ice-core records: refining and extending the INTIMATE event stratigraphy. *Quaternary Science Reviews*. 2014;106:14-28. doi:10.1016/j.quascirev.2014.09.007
38. Goodfriend GA. Radiocarbon age anomalies in shell carbonate of land snails from semi-arid areas. *Radiocarbon*. 1987;29(2):159-167. doi:10.1017/S0033822200056915
39. Pigati JS, Rech JA, Nekola JC. Radiocarbon dating of small terrestrial gastropod shells in North America. *Quaternary Geochronology*. 2010;5(5):519-532. doi:10.1016/j.quageo.2010.01.001
40. Újvári G, Molnár M, Páll-Gergely B. Charcoal and mollusc shell 14C-dating of the Dunaszekcso loess record, Hungary. *Quaternary Geochronology*. 2016;35:43-53. doi:10.1016/j.quageo.2016.05.005
41. Durand N, Monger HC, Canti MG. Calcium carbonate features. In: Stoops G, Marcelino V, Mees F, eds. *Interpretation of micromorphological features of soils and Regoliths*. Amsterdam: Elsevier; 2010:149-194. doi:10.1016/B978-0-444-53156-8.00009-X
42. Jaillard B, Guyon A, Maurin AF. Structure and composition of calcified roots, and their identification in calcareous soils. *Geoderma*. 1991;50(3):197-210. doi:10.1016/0016-7061(91)90034-Q
43. Ballantyne CK, Harris C. *The Periglaciation of Great Britain*. Cambridge: Cambridge University Press; 1994. 330 pp.
44. Harvey AM. Factors influencing quaternary alluvial fans development in Southeast Spain. In: Rachocki AM, Church M, eds. *Alluvial fans: A field approach*. Wiley; 1990:247-269.

45. Rousseau DD, Keen DH. Malacological records from the Upper Pleistocene at Portelet (Jersey, Channel Islands): comparisons with western and Central Europe. *Boreas*. 1989;18:61-66.
46. Limondin-Lozouet N, Antoine P. Palaeoenvironmental changes inferred from malacofaunas in the Lateglacial and Early Holocene fluvial sequence at Conty (northern France). *Boreas*. 2001;30(2):148-164. doi:10.1080/030094801750203161
47. Limondin N. *Paysages et climats quaternaires par les mollusques continentaux*Thèse de Doctorat d'Université. Université de Paris I-Panthéon Sorbonne; 1990. 419 p.
48. Limondin N. Late-glacial and Holocene Malacofaunas from archaeological sites in the Somme Valley (North France). *J Archaeol Sci*. 1995;22(5):683-698. doi:10.1016/S0305-4403(95)80154-5
49. Pastre JF, Limondin-Lozouet N, Leroyer C, Ponel P, Fontugne M. River system evolution and environmental changes during the Lateglacial in the Paris Basin (France). *Quaternary Sciences Reviews*. 2003;22(20):2177-2188. doi:10.1016/S0277-3791(03)00147-1
50. Revel JC. *Formation des sols sur marnes, étude d'une chronoséquence et d'une toposéquence complexe dans le Terrefort toulousain*Thèse de Doctorat. Université Paul Sabatier et Institut National Polytechnique de Toulouse; 1982. s.
51. Bertran P, Allenet G, Fourloubey C, et al. Paléoenvironnements tardiglaciaires en Aquitaine: la séquence alluviale de la Brunetière (Bergerac, France). *Quaternaire*. 2009;20(2):161-193.
52. Magnin F. Les distributions pléistocène et actuelle de *Trochoidea (Xeroclausa) geyeri* (Soós, 1926) (Gastropoda, Helicidae) dans le Sud-Est de la France: un exemple de disjonction d'aire liée au réchauffement post-glaciaire. *Bulletin de la Société Géologique de France*. 1989;8(4):779-786. doi:10.2113/gssgfbull.V.4.779
53. Ensom T, Makarieva O, Morse P, Kane D, Alekseev V, Marsh P. The distribution and dynamics of aufeis in permafrost regions. *Permafrost and Periglacial Processes*. 2020;31(3):383-395. doi:10.1002/ppp.2051
54. Hall DK. Mineral precipitation in north Slope River icings. *Arctic*. 1980;33(2):343-348.
55. Harden D, Barnes P, Reimnitz E. Distribution and character of naleds in Notheastern Alaska. *Arctic*. 1977;30(1):28-40. doi:10.14430/arctic2681
56. Lauriol B, Cinq-Mars J, Clark ID. Localisation, genèse et fonte de quelques naleds du nord du Yukon (Canada). *Permafrost and Periglacial Processes*. 1991;2(3):225-236. doi:10.1002/ppp.3430020306
57. Van Everdingen RO. Frost blisters of the bear rock spring area near Fort Norman, N.W.T. *Arctic*. 1982;35(2):243-265. doi:10.14430/arctic2324
58. Liu W, Fortier R, Molson J, Lemieux JM. A conceptual model for talik dynamics and icing formation in a river floodplain in the continuous permafrost zone at Salluit, Nunavik (Quebec), Canada. *Permafrost and Periglacial Processes*. 2021;32(3):468-483. doi:10.1002/ppp.2111
59. Pollard WH, van Everdingen RO. Formation of seasonal ice bodies. In: Dixon J.C., Abrahams A.D. eds. *Proceedings 22nd Binghamton Symposium in Geomorphology*. John Wiley and Sons, Chichester; 1992:282-304.
60. Marlin C, Dever L, Courty MA, Vachier P. Chemistry and isotopes of soil water during freezing. In: Kharaka et Maest, ed. *Water-rock interaction*. Balkema, Rotterdam; 1992:731-735.
61. Bukowska-Jania E. The role of glacier system in migration of calcium carbonate on Svalbard. *Polish Polar Research*. 2007;28(2):137-155.
62. Clark ID, Lauriol B. Kinetic enrichment of stable isotopes in cryogenic calcite. *Chem Geol*. 1992;102(1-4):217-228. doi:10.1016/0009-2541(92)90157-Z
63. Lacelle D, Lauriol B, Clark ID. Effect of chemical composition of water on the oxygen-18 and carbon-13 signature preserved in cryogenic carbonates, Arctic Canada: implications in paleoclimatic studies. *Chem Geol*. 2006;234(1-2):1-16. doi:10.1016/j.chemgeo.2006.04.001
64. Bowen GJ, Wilkinson B. Spatial distribution of $\delta^{18}O$ in meteoric precipitation. *Geology*. 2002;30(4):315-318. doi:10.1130/0091-7613(2002)0302.0.CO;2
65. Clark ID, Lauriol B. Aufeis of the Firth River Basin, Northern Yukon, Canada: Insights into permafrost hydrogeology and karst. *Arctic and Alpine Research*. 1997;29(2):240-252.
66. Bertran P, Font M, Giret A, Manchuel K, Sicilia D. Experimental soft-sediment deformation caused by fluidization and intrusive ice melt in sand. *Sedimentology*. 2018;66(3):1102-1117. doi:10.1111/sed.12537
67. Kim ST, O'Neil JR. Equilibrium and nonequilibrium oxygen isotope effects in synthetic carbonates. *Geochim Cosmochim Acta*. 1997;61(16):3461-3475. doi:10.1016/S0016-7037(97)00169-5

SUPPORTING INFORMATION

Additional supporting information can be found online in the Supporting Information section at the end of this article.

How to cite this article: Bertran P, Couchoud I, Charlier K, et al. Last Glacial Maximum cryogenic calcite deposits in an alluvial fan at Villetoureix, southwest France. *Permafrost and Periglac Process*. 2023;1-15. doi:10.1002/ppp.2183